Fibers and Polymers 2014, Vol.15, No.6, 1242-1250 DOI 10.1007/s12221-014-1242-4

Scalable Preparation of Multiscale Carbon Nanotube/Glass Fiber Reinforcements and Their Application in Polymer Composites

Ke Peng[1,2], Yan-Jun Wan[1], Dong-You Ren[2], Qing-Wen Zeng[2], and Long-Cheng Tang[1]*

[1]*Key Laboratory of Organosilicon Chemistry and Material Technology of Ministry of Education, Hangzhou Normal University, Hangzhou 310012, China*

[2]*Chongqing Polycomp International Corporation, Chongqing 400082, China*

(Received October 12, 2013; Revised December 3, 2013; Accepted December 22, 2013)

Abstract: The introduction of carbon nanotubes (CNTs) into conventional fiber to construct a hierarchical structure in polymer composites has attracted great interest owing to their merits of performance improvement and multiple functionalities. However, there is a challenge for realizing the scalable preparation of the multi-scale CNT-glass fiber (CNT-GF) reinforcements in practical application. In this work, we present a simple and continuous method of the mass production of multiscale CNT-glass fiber (CNT-GF) reinforcements. Scanning electron microscopy and thermo gravimetric analysis indicated ~1.0 wt% CNTs were highly dispersed on the whole fiber surface through a facile surfactant-assisted process. Such hybrid CNT-GF fillers were found to effectively enhance the stiffness, strength and impact resistance of polypropylene polymer. Increased storage modulus, glass transition temperature and crystallization temperature of the composites filled with the CNT-GF fillers were also observed in the differential scanning calorimetry and dynamic mechanical analysis compared with the composites containing the pristine GF fillers. Fracture surface analysis revealed enhanced interfacial quality between CNT-GF and matrix, which is likely responsible for improved performance of the hierarchical polymer composites.

Keywords: Glass fibers, Carbon nanotubes, Polymer-matrix composites (PMCs), Mechanical properties, Electron microscopy

Introduction

Advanced fiber-reinforced polymer composites (FRPs) are known to possess superior performance and their use in many structural applications continues to expand. However, most FRPs are susceptible to micro- and nano- scale damages, such as interfacial debonding, matrix cracking and fiber breakage. Premature failure may take place at the weak fiber/matrix interface and thus result in the reduced properties of FRPs. Therefore, a composite made from a well-suited matrix and a strong fiber may not necessarily produce a strong material because the fiber/matrix interface is equally important in determining the final performance of the composite [1].

Carbon nanotubes (CNTs) have exceptional mechanical and physical properties such as high modulus and strength that make them as ideal reinforcements for polymer composites [2-5]. In the past decade, in order to realize the effective "bridge" at the fiber/matrix interface, the introduction of CNTs into the conventional fiber to create a hierarchical reinforcement structure in polymer composites has attracted great interest [6-17]. To date, three methods have been mainly developed to prepare the multiscale CNT-fibers: (i) direct growth of CNTs on the fiber surface by using chemical vapor deposition (CVD) [11,18-21], (ii) substitution of sizing polymer resin by a CNT-polymer mixture [22-26], and (iii) deposition of CNTs on the fiber surface by electrophoretic deposition (EPD) [7,27-31]. These methods have been proven to effectively improve the interface between fiber and matrix, which in turn enhances the mechanical performance of hierarchical polymer composites [32]. However, there are still some drawbacks and limitations in practical applications. The CVD method (i) has several advantages in terms of dispersion and controlled growth of the CNTs on the fiber surface. Whereas the use of high temperature and excessive chemical treatments during CVD process would impose serious limitations such as scalability and degradation of the fibers [33]. In case of the method (ii), this approach is the most widely used in manufacturing of hierarchical composites owing to its practicality and scalability. But the CNT dispersion and the excessively increased viscosity of the CNT/polymer mixture issues, especially at nanotube loadings higher than 1.0 wt%, are not completely resolved [34,35].

Comparatively, the EPD method (iii) shows potential and promising in terms of practicality, cost-effectiveness and scalability [7,36,37]. Recently, Guo and Lu [30] placed the carbon fiber (CF) tows (as the deposition electrode) in the middle of the two metallic electrodes and continuously prepared the hybrid CNT-CF fillers. Unlike CFs, glass fibers (GFs) cannot be used as deposition electrode directly due to their insulating property. Zhang [27] and his coworkers tried to use the two parallel copper plates as cathode and anode to fabricate the multiscale CNT-GF fillers. The results revealed, however, that the EPD technique was still very difficult to achieve a homogeneous distribution of the CNTs on the round GFs because one side of the fiber was always preferentially exposed to the 'depositing' CNTs. Considering the fact that the price of commercial GFs is much lower than that of CFs, the fabrication of multiscale CNT-GF fillers

*Corresponding author: lctang@hznu.edu.cn

should present more attractive and compatible with industry practice. Unfortunately, to the best of our knowledge, few studies have been performed regarding the simple and scalable method for preparing multi-scale CNT-GF reinforcements.

In this paper, a simple and continuous preparation of multiscale CNT-GF fillers was developed through a facile surfactant-assisted process, and the fabrication of the hybrid CNT-GF reinforced polypropylene (PP) composites was also reported. The tensile and thermal-mechanical properties of hierarchical PP composites were measured to evaluate the reinforcing effect of the multiscale CNT-GF fillers. Moreover, the microscopic morphologies and fracture behaviors of the polymer composites were characterized and discussed.

Experimental

Materials

The polymer matrix used in this work was commercial grade PP with a melting temperature of 165 °C and molecular weight of about 69000 (SF35, China National Petroleum Corporation). Commercially available GFs were produced from Chongqing Polycomp International Corporation and had a commercial sizing with PP film former and γ-aminopropyl-triethoxysilane (γ-APS). The multi-walled carbon nanotubes (MWCNTs, Timestub™, Chengdu Organic Chemicals Co., Ltd.) were produced in a high-yield catalytic process with a purity of carbon content more than 95 wt%. The length of MWCNTs was about 50 μm and their outer diameters ranged from 20 to 30 nm. Non-ionic amphiphilic surfactant, polyoxyethylene octyl phenyl ether (POPE, Triton X-100) with the critical micelle concentration (CMC) value of 0.2 mM at 25 °C, was purchased from Acros Organics.

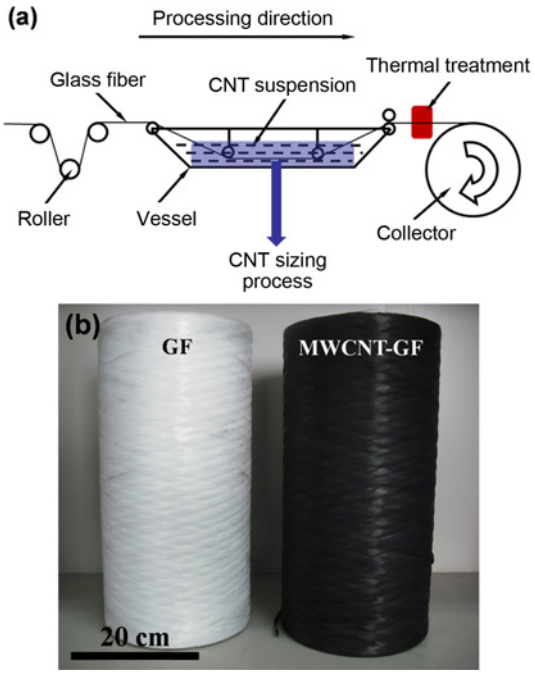

Figure 1. (a) Schematic for continuous preparation of multiscale MWCNT-GF and (b) typical digital picture of pristine GFs as produced and MWCNT-GF reinforcements.

Preparation of Multiscale MWCNT-GF Reinforcements

The preparation process of multiscale MWCNT-GF reinforcements was introduced as following (see Figure 1(a)). First, we prepared a stable CNT suspension. For this purpose, the non-ionic POPE surfactant was used in this study. According to the previous work [38], ~1 g of pristine MWCNTs and ~5 g of surfactant were added into ~1000 m*l* of water. After sonicating for ~2 h in a sonicator bath, the POPE molecules were absorbed by the highly dispersed MWCNTs through physical absorptions [39]. Thus a stable and uniform suspension of surfactant-treated MWCNTs was obtained. Then, it was done by drawing the GFs through the above stable MWCNT/water solution at ~15 m/min. After the sizing procedure, the GF tows were quickly treated by thermal process, and then wound up on a roll. Figure 1(b) presents the digital image of the pristine fibers and multiscale MWCNT-GF fillers produced. Moreover, such continuous fiber rovings were chopped into strands with 3 mm in length for filling the PP matrix.

Fabrication of Hierarchical Polymer Composites

The composites were prepared by feeding the short MWCNT-GFs into the polymer melt using a twin screw extruder. The six heating zones were set to 230 °C, 230 °C, 220 °C, 220 °C, 220 °C and 220 °C and the screw speed was set at 200 rpm. The compounded extrudates were quenched in water and cooled in air till ambient temperature. Then the extruded strands were chopped into granules and dried. All the specimens were injection molded into dumbbell-shaped tensile bars under identical conditions using a twin screw injection molding machine with a barrel temperature of 210-230 °C. For comparison, both the pure PP and GF/PP composites were also prepared according to the above procedure described for MWCNT-GF/PP composites.

Characterization

The structures of both GF and MWCNT-GF fillers were examined by a scanning electron microscopy (SEM, HITACHI S-4800). Thermo gravimetric analysis (TGA) of various fillers was conducted by TA Instruments Q500 with a heating rate of 20 °C/min under air atmosphere. Dynamic mechanical thermal analysis (DMTA) was made in tensile mode using a Dynamic Mechanical Analyzer (NETZSCH, DMA 242), which was performed in the temperature range from −30 °C to 150 °C at a constant heating rate of 3 °C/min and a fixed frequency of 1 Hz. Differential scanning calorimetry (DSC) was applied to determine the crystallization temperature (T_c) and the degree of crystallinity (X_c) of the PP-based composites (Q100, TA Instruments). All scans were performed in a nitrogen atmosphere. The X_c was calculated according to the

relationship:

$$Xc = Hf_w^o / Hf^o \times 100\ \%$$

where Hf^o=209 J/g is the heat of fusion of 100 % crystalline material and Hf_w^o is the normalized heat of fusion of the sample.

The notched impact tests were performed with an impact tester (XCJ-5, Chengde Testing Machine Co., Ltd.) according to ISO 179-1. Tensile tests were performed at a crosshead speed of 1.0 mm/min at room temperature using an Ametek Ls100plus, according to the ASTM D-638. At least five specimens of each composition were tested. The microscopy analysis of fracture surfaces was sputtered with gold for 30 s and observed under SEM and optical microscopy (TOM, Nikon Eclipse LV100 POL).

Results and Discussion

Morphology and Structure of Multiscale CNT-GF Reinforcements

Characterization of the GFs before and after MWCNT sizing process was performed using SEM (Figure 2). As shown in Figure 2(a), the as-received GFs with the commercial sizing are about 15 μm in diameter and exhibit relatively smooth surface along their axis (see the inset). By comparison, the surface morphologies of the GF show some obvious changes after the sizing process. Fairly good distribution of MWCNTs can be observed on each individual fiber, forming a rough surface (see Figures 2(b) and 2(c)). This is quite different from the relatively smooth surface of fiber after sizing the epoxy resin [40-43]. Moreover, it can be clearly found that the MWCNTs in Figure 2(d) are well distributed on the whole fiber surface, and even induce an interconnected network.

It is worth noting that, in other work [44], although the GFs sized by the CNT/epoxy mixture were favorable to improve the properties of the fiber/matrix interface, they tend to cause a non-uniform film on the fiber surface probably due to the excessively increased viscosity. However, such issue is absent in the present work for the multiscale MWCNT-GF reinforcements. Similar CNT-CF fillers were continuously prepared by Lu *et al.* [30,31] through using the EPD method, which has been proven to improve the fiber/matrix interfacial quality effectively [45].

Thermo Gravimetric Analysis of Various Fillers

TGA analysis can be utilized to investigate the thermal stability of various fillers and quantify the amount of MWCNTs on the GF surface in the hybrid MWCNT-GF fillers. Normally, the pristine fibers present good thermal stability even at high temperature of 800 ^oC (see Figure 3). A weight loss of ~0.8 % was observed in the temperature range from 300 to 550 ^oC due to a thermally stripped sizing of PP film former and γ-APS. In case of the as-received MWCNT fillers, the major mass loss occurs at approximately 550 ^oC under air atmosphere, suggesting that the nanotube structure started to oxidize and generate CO and CO_2 gases.

Comparatively, although the multiscale MWCNT-GF fillers exhibit a similar thermal stability as the pristine GFs, some differences can be still observed. First, compared to the pristine fiber, a slightly more weight loss (~0.4 wt%) of MWCNT-GF is observed between 350 and 550 ^oC, which is

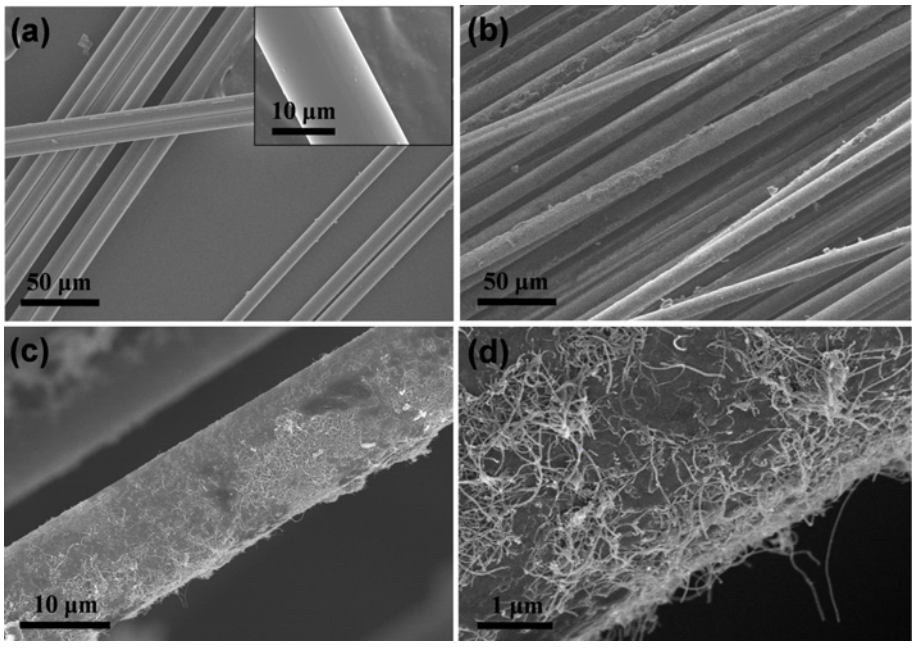

Figure 2. SEM images of (a) pristine GF, and (b), (c) and (d) MWCNT-GF observed under different magnifications.

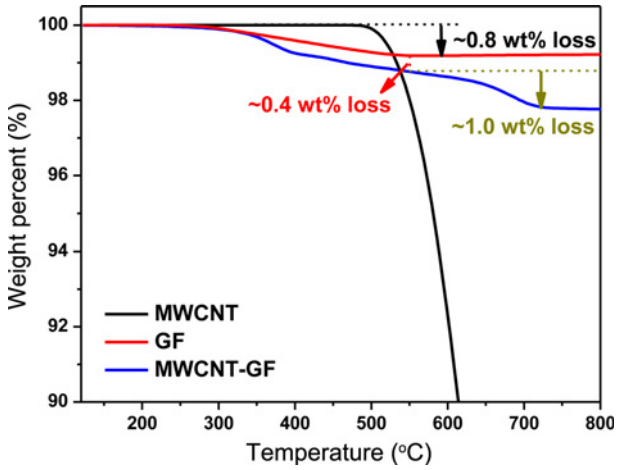

Figure 3. TGA curves of various fillers: pristine GF, MWCNT and MWCNT-GF.

likely attributed to degradation of the surfactant POPE molecules. Normally, the hydrophilic regions of nonionic POPE surfactants interact with polar solvent molecules, and the hydrophobic regions can adsorb onto nanofiller surfaces [46-48]. During the sizing process, a small amount of POPE could assemble around MWCNTs and thus form a large solvation shell from the hydrophilic moieties [49-51] (Most of surfactant should be dissolved in the aqueous dispersion). Moreover, the MWCNT-GF fillers also present further mass loss above 550 °C when compared to the GFs, which is consistent with the temperature of oxidization of MWCNTs. It implies that the amount of MWCNTs on the fiber surface in the mutiscale fillers seems to be only ~1.0 wt%, as indicated in Figure 3.

Dynamic Mechanical Properties of the Composites

Dynamic mechanical analysis can characterize the viscoelastic properties of the materials and determine the information of storage modulus and loss factor (tan delta) within the measured temperature range [52-54]. The storage modulus spectra of pure PP and its composites are shown in Figure 4(a). As expected, the incorporation of the GFs results in a significant increase in the storage modulus in the whole temperature range when compared to the pure PP. It can well be explained by the reinforcing effect of the fiber leading to increased

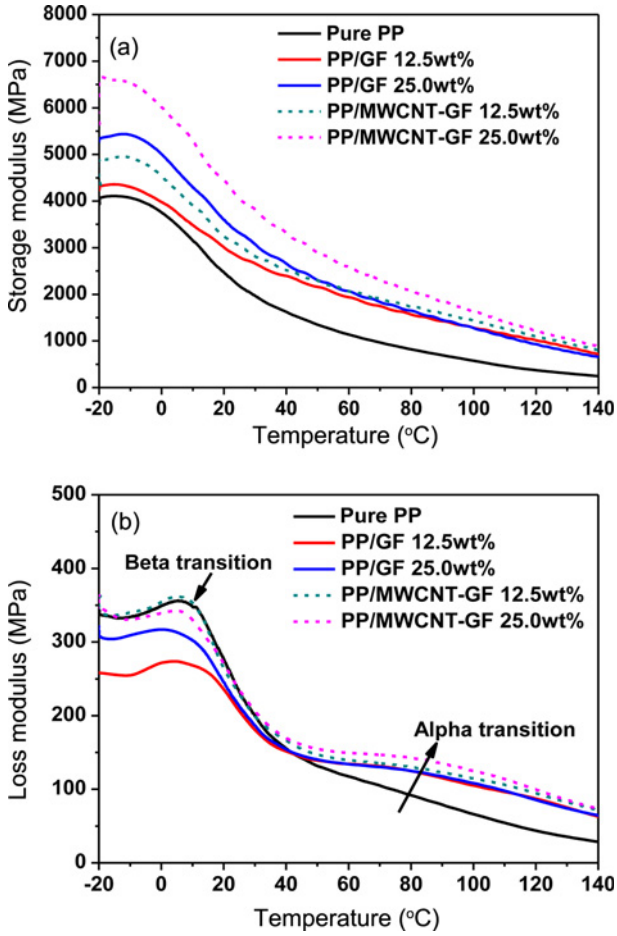

Figure 4. DMTA curves of neat PP and its composites; (a) storage modulus and (b) loss modulus.

stiffness. In comparison, the presence of hybrid MWCNT-GF fillers produces the higher modulus enhancement of the PP composites, suggesting increased stiffness of PP composites.

Figure 4(b) shows the loss modulus spectra of pure PP and its composites. Two major features can be seen. First, a low transition temperature of PP composites i.e. the glass transition temperature (T_g) is observed between 0 °C and 10 °C for all composites studied. Clearly, the T_g value of the MWCNT-GF reinforced PP composites shows slightly higher than that of the GF reinforced PP composites (see Table 1). At the fixed content of 25.0 wt%, the T_g value (~4.9 °C) of the

Table 1. The mechanical properties, T_g and T_c values of pure PP and its composites

Sample	Elastic modulus (GPa)	Tensile strength (MPa)	Elongation at break (%)	T_g (°C)	T_c (°C)
Pure PP	1.91±0.11	35.12±0.51	160.37±4.43	5.1±0.3	115.5
GF/PP, 12.5 wt%	3.33±0.10	65.15±0.66	3.05±0.15	4.1±0.5	120.2
GF/PP, 25.0 wt%	5.44±0.21	76.48±1.12	2.22±0.21	0.6±0.4	121.2
MWCNT-GF/PP, 12.5 wt%	3.86±0.10	68.92±1.34	2.07±0.08	4.9±0.3	121.3
MWCNT-GF/PP, 25.0 wt%	6.22±0.51	79.83±1.09	1.68±0.11	4.9±0.4	121.9

multiscale composites exhibits about 4.3 °C much higher than that of the GF/PP composites (~0.6 °C). On the other hand, a second transition is found in the range of 60-90 °C (see Figure 4(b)), which corresponds to the alpha transition [55]. Unlike the unclear alpha transition of pure PP, it becomes relatively distinct for the composites, especially for the MWCNT-GF/PP composites. It is well established that the alpha transition in the semicrystalline PP is associated with both the transcrystalline relaxation and sliding of tied macromolecules within crystalline blocks of PP [55,56]. The slight change of peak intensity of PP composites implies that the lamellar movement in the crystalline phase is strongly restricted by addition of the multiscale MWCNT-GF fillers.

Polymer Crystallinity

In order to evaluate the nucleating role of the sizing CNTs on fiber surface, the crystallization temperature of PP composites was measured by DSC. Calculations of X_C of the composites were examined to determine whether the presence of GF and MWCNT-GF fillers interferes with the polymer crystalline phase. Examples of the DSC traces are shown in Figure 5 for a neat PP sample and for PP composites containing pristine GF or MWCNT-GF fillers, and the results of the T_c values are summarized in Table 1 for all the composites.

On the basis of the DSC results (Table 1), it can be concluded that the presence of polymer sized glass fibres with or without MWCNTs on the fiber surface tend to raise T_c by about 4-6 °C when compared to the pure PP, indicating a higher nucleation ability of the matrix. Although the polymer sized on the fiber increases the T_c value (Table 1), the MWCNT-GF reinforced PP composites present much slightly higher T_c values than those of the corresponding GF reinforced PP composite, suggesting accelerated nucleation

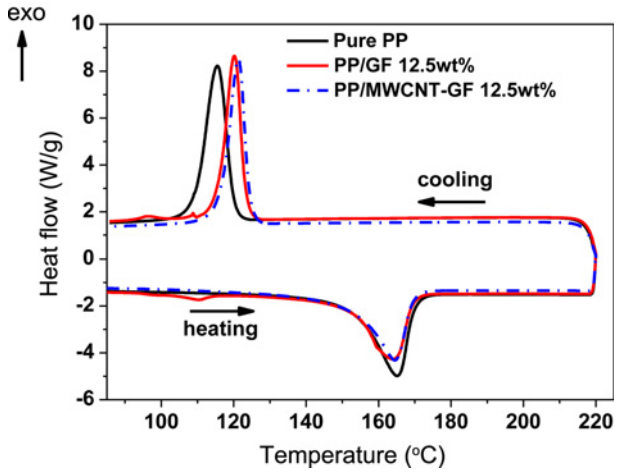

Figure 5. DSC traces for pure PP and PP composites containing 12.5 wt% of pristine GF and MWCNT-GF fillers. The samples were heated from room temperature to 220 °C to detect the melting process, followed by cooling to 80 °C in order to observe the polymer crystallization. The heating/cooling rate is 20 °C/min.

activity produced by the addition of MWCNTs [57]. Moreover, incorporation of both GF and MWCNT-GF fillers into PP matrix results in decreased X_c (from ~0.685 to ~0.641 for pristine GF and ~0.676 for MWCNT-GF fillers at 12.5 wt%) probably due to the presence of fibers acting as diluent in the matrix [58]. However, the MWCNT-GF/PP composites still show much higher X_c value compared with the GF/PP composites. Numerous MWCNTs that were well distributed on the fiber surface (see Figure 2(d)) probably promoted the folding of some polymeric chains during the crystallization process, and as a result enhanced the X_c value [59].

Mechanical Properties of the Composites

The representative tensile stress-strain curves of pure PP and its composite are shown in Figure 6, and their key mechanical properties are summarized in Table 1. In general, the pure PP shows a ductile type of curve and the strain of failure is about 160 % (Figure 6(a)). By comparison, both pristine GF and MWCNT-GF fillers decrease the elongation at break significantly. A linear deformation at low stress and nonlinear deformation at high stress without a yielding process can be observed in these two systems (Figure 6(a)), showing a typical brittle fracture.

As shown in Table 1 and Figure 6(b), the unfilled PP has the elastic modulus of about 1.91 GPa. Addition of GF increases the elastic modulus of the GF/PP samples significantly, e.g. about 185 % (~5.44 GPa) improvement at 25.0 wt%. In contrast, incorporation of the 25.0 wt% multiscale MWCNT-GF fillers into PP results in much higher improvement of about 226 % (~6.22 GPa) in the elastic modulus. The tensile strength of the composite samples gives a similar tendency to the elastic modulus (see Figure 6(c)). The 25.0 wt% GF and MWCNT-GF fillers produce about 118 % and 127 % increase (form 35.12±0.51 for pure PP to 76.48±1.14 and 79.83±1.09 MPa for the GF/PP and MWCNT-GF/PP composites) in tensile strength, respectively. Moreover, both the GF and MWCNT-GF can also provide a dramatic increase in the notched impact strength of PP matrix (see Figure 6(d)), although the MWCNT-GF/PP samples present a slight decrease in impact strength compared to the corresponding GF/PP samples, e.g. 13.8±0.2 kJ/m^2 for the GF and 12.8±0.3 kJ/m^2 for the MWCNT-GF at 25.0 wt% (Table 1). Thereby, it can be found that the addition of multiscale MWCNT-GF fillers effectively improve the modulus and strength and impact strength of PP polymer. This would provide a platform to develop the high performance hierarchical polymer composites for some engineering applications.

Fracture Surface Analysis

In order to investigate the acting deformation mechanisms responsible for improved tensile properties, fracture surfaces of the composite samples were examined and shown in Figure 7. Normally, two obvious features i.e. many GF segments and some voids after fiber pull-out from the matrix

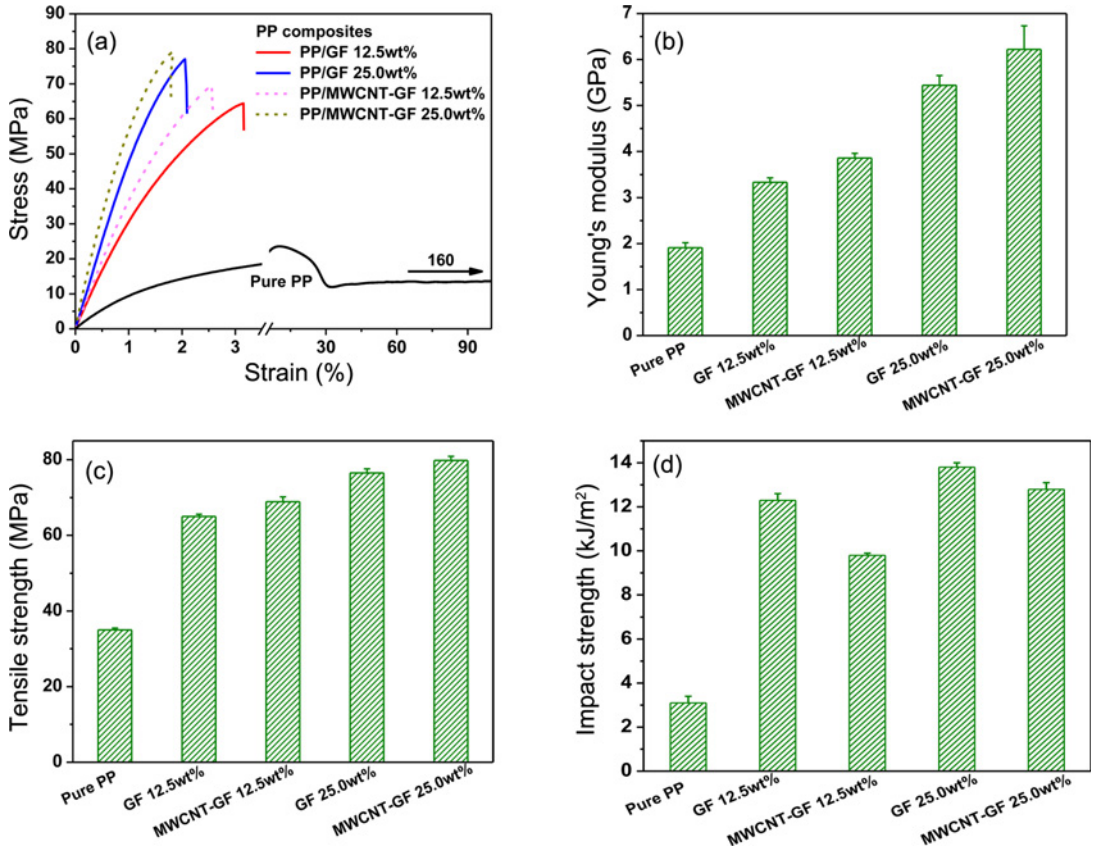

Figure 6. Mechanical properties of pure PP and its composites; (a) typical stress-strain curves, (b) elastic modulus, (c) tensile strength, and (d) notched impact strength.

can be identified on the fracture surface for both GF/PP and MWCNT-GF/PP composites (see Figures 7(a) and 7(b)). However, some obvious differences can be still detected between these two systems. First, careful observations between Figures 7(a) and 7(b) suggest that the length of fiber segments left on the fracture surface in the GF/PP composites seems to be much longer than that in the MWCNT-GF/PP composites, which is related with the fiber/matrix interfacial quality. The strong interfacial bonding facilitates the stress transfer from the matrix to the fiber and even induces the fiber breakage in term of short residual length on the fracture surface. Second, unlike the smooth and clean surface of GF in the GF/PP system (see the black arrows in Figure 7(c)), many residues of polymer and nanotubes can be observed on the surface of MWCNT-GF (see the black arrows in Figure 7(d)), implying that the PP molecule chains may wrap the nanoscale CNTs during the high shear process. Similar phenomenon of PP polymer residue on the CNT-coated GF surfaces was previously observed in Ref. [60], indicating the enhanced adhesion between the fiber and the matrix.

In fact, the interfacial quality between GF and PP matrix can be clearly observed on the fracture surface. As indicated by the white arrows in Figure 7(c), some obvious gaps between matrix and fiber can be clearly seen in the GF/PP composites. Normally, under the high tensile stress field, the GFs usually slip from the PP matrix during the fracture process due to the weak adhesion between fiber and matrix. Consequently, the debonding between fiber and matrix may occur. In contrast, the interface between GF and matrix is significantly improved after the presence of MWCNTs since no obvious gaps between MWCNT-GF and PP matrix are observed in the Figure 7(d) (see the white arrows). The high magnified images of fracture surface can further demonstrate these phenomena (see white arrows). In addition, in the MWCNT-GF/PP composites (Figure 7(f)), although the rough fracture surface of the composites is difficult for us to directly examine the roles of MWCNTs, some MWCNTs are still observed to bridge the propagating crack between PP and fiber (see the white arrow in the inset). This suggests that the rough surface structure of the multiscale MWCNT-GF fillers in Figure 2(d) could produce the mechanical interlocking of particles to improve the fiber/matrix interfacial quality [37], which should be responsible for the highly improved stiffness and strength of the MWCNT-GF/PP composites.

As is well known, in the short fiber reinforced polymer (SFRP) composites, the fiber failure mode relies on its

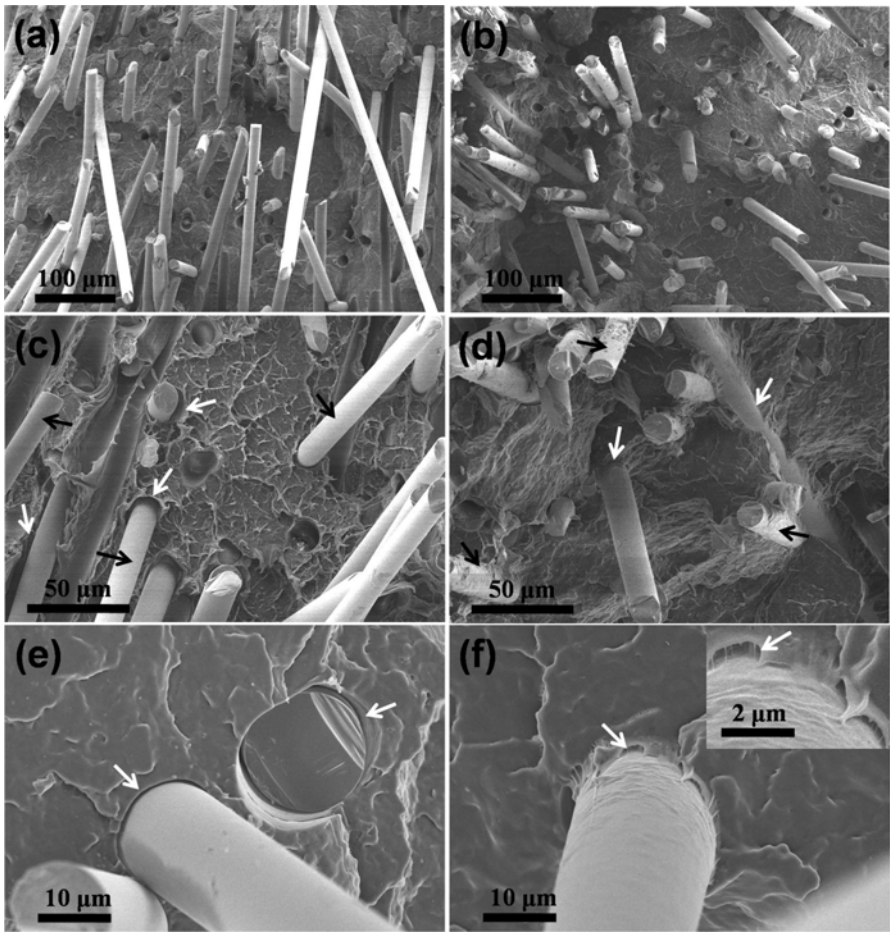

Figure 7. SEM images of tensile fracture surface of PP composites with: (a), (c) and (e) 25. 0 wt% GF; (b), (d) and (f) 25.0 wt% MWCNT-GF.

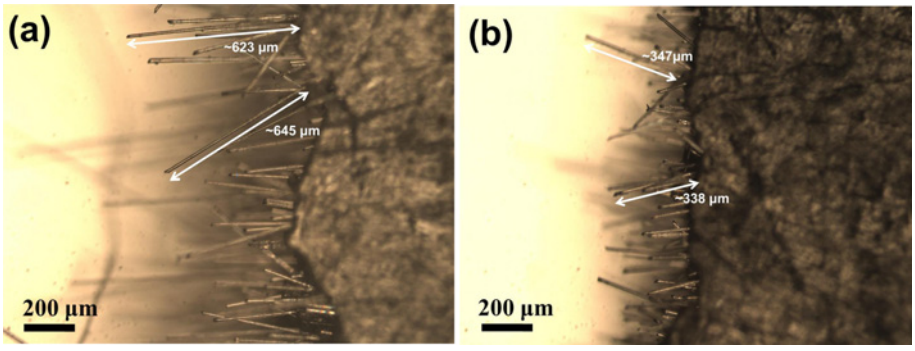

Figure 8. Optical micrographs of the polished sections of specimens after tensile tests, perpendicular and near to the fracture planes, of PP composites containing; (a) 25.0 wt% GF and (b) 25.0 wt% MWCNT-GF (The white arrows indicate the maximum fiber pullout lengths measured from the fracture surfaces of the composite samples).

critical length (l_c) [61-64]. The fibers shorter than l_c should be pulled out of polymer matrix during composite fracture; while they tend to be broken if their embedded segment lengths at both fracture sections are larger than half of their critical length [65]. In fact, the l_c value is strongly dependent on the interfacial quality between fiber and matrix [66]. Normally, the l_c value can be approximately obtained by doubling the average of the maximum fiber pullout lengths from the fracture surfaces of the samples since the maximum fiber pullout length should be equivalent to half of the

critical length in principle [65,67]. Pullout lengths of the 10 maximum fiber pullout lengths can be averaged as half of the critical fiber length [68]. According to the fracture surface observations by optical microcopy (see Figures 8(a) and 8(b)), the critical fiber length was obtained to be ~1296 and ~682 μm for the GF/PP and MWCNT-GF/PP composites, respectively. Considering the similar process of the composites, the reduced critical fiber length after the use of MWCNTs suggests that the multiscale MWCNT-GF fillers produced in this work are effective to improve the fiber/matrix interface, which is consistent with the fracture surface observations.

Conclusion

In this work, we present a simple and scalable method of the mass production of CNT-GF reinforcements, and investigated their relative reinforcing effect and fracture behaviors of the hierarchical polymer composites. Based on a facile surfactant-assisted process, the scalable preparation of multiscale MWCNT-GF reinforcements was developed. Fairly good distribution of MWCNTs was observed on each individual fiber. Thermo gravimetric analysis suggested that the amount of MWCNTs on the fiber surface in the mutiscale fillers was about 1.0 wt%. Tensile and impact tests indicated that such multiscale MWCNT-GF reinforcements effectively improved the tensile modulus and strength and impact strength of PP composites with significant loss in elongation at break. The composites with the MWCNT-GF fillers also showed higher glass transition temperature and crystallization temperature than the composites with the corresponding pristine GF fillers from DMTA and DSC analysis. The micrographs of fracture surfaces revealed that the interfacial quality between GF and PP matrix was improved after the MWCNTs sizing process, which is likely responsible for the improved mechanical properties of the hierarchical PP-based composites. The reduced critical fiber length after the presence of MWCNTs on the fiber surface was observed for the MWCNT-GF/PP composites, which further demonstrated the enhanced fiber/polymer interfacial quality in the hierarchical polymer composites.

Acknowledgements

We gratefully acknowledge the support from the National Natural Science Foundation of China (51203038), the Zhejiang Provincial Natural Science Foundation of China (LQ13E030009), the Scientific Research Fund of Zhejiang Provincial Education Department (Y201224314) and the Starting Foundation for Scholars of Hangzhou Normal University (2012QDL022).

References

1. Y. R. Lin, G. Ehlert, and H. A. Sodano, *Adv. Funct. Mater.*, **19**, 2654 (2009).
2. F. H. Gojny, M. H. G. Wichmann, U. Kopke, B. Fiedler, and K. Schulte, *Compos. Sci. Technol.*, **64**, 2363 (2004).
3. E. T. Thostenson and T. W. Chou, *Carbon*, **44**, 3022 (2006).
4. L. C. Tang, H. Zhang, J. H. Han, X. P. Wu, and Z. Zhang, *Compos. Sci. Technol.*, **72**, 7 (2011).
5. L. C. Tang, Y. J. Wan, K. Peng, Y. B. Pei, L. B. Wu, L. M. Chen, L. J. Shu, J. X. Jiang, and G. Q. Lai, *Compos. Part A-Appl. S.*, **45**, 95 (2013).
6. F. H. Gojny, M. H. G. Wichmann, B. Fiedler, W. Bauhofer, and K. Schulte, *Compos. Part A-Appl. S.*, **36**, 1525 (2005).
7. E. Bekyarova, E. T. Thostenson, A. Yu, H. Kim, J. Gao, J. Tang, H. T. Hahn, T. W. Chou, M. E. Itkis, and R. C. Haddon, *Langmuir*, **23**, 3970 (2007).
8. M. Kim, Y. B. Park, O. I. Okoli, and C. Zhang, *Compos. Sci. Technol.*, **69**, 335 (2009).
9. L. M. Gao, E. T. Thostenson, Z. Zhang, and T. W. Chou, *Adv. Funct. Mater.*, **19**, 123 (2009).
10. T. W. Chou, L. Gao, E. T. Thostenson, Z. Zhang, and J. H. Byun, *Compos. Sci. Technol.*, **70**, 1 (2010).
11. H. Qian, A. Bismarck, E. S. Greenhalgh, and M. S. P. Shaffer, *Compos. Part A-Appl. S.*, **41**, 1107 (2010).
12. B. C. Wang, X. Zhou, and K. M. Ma, *Compos. Part B-Eng.*, **46**, 123 (2013).
13. H. Qian, A. R. Kucernak, E. S. Greenhalgh, A. Bismarck, and M. S. Shaffer, *ACS Appl. Mater. Interfaces*, **5**, 6113 (2013).
14. N. De Greef, L. Gorbatikh, A. Godara, L. Mezzo, S. V. Lomov, and I. Verpoest, *Carbon*, **49**, 4650 (2011).
15. A. Godara, L. Mezzo, F. Luizi, A. Warrier, S. V. Lomov, A. W. van Vuure, L. Gorbatikh, P. Moldenaers, and I. Verpoest, *Carbon*, **47**, 2914 (2009).
16. J. Rausch, R. C. Zhuang, and E. Mader, *Materials Technology*, **24**, 29 (2009).
17. M. Li, Y. Gu, Y. Liu, Y. Li, and Z. Zhang, *Carbon*, **52**, 109 (2013).
18. E. T. Thostenson, W. Z. Li, D. Z. Wang, Z. F. Ren, and T. W. Chou, *J. Appl. Phys.*, **91**, 6034 (2002).
19. Q. J. Gong, H. J. Li, X. Wang, Q. G. Fu, Z. W. Wang, and K. Z. Li, *Compos. Sci. Technol.*, **67**, 2986 (2007).
20. K. L. Kepple, G. P. Sanborn, P. A. Lacasse, K. M. Gruenberg, and W. J. Ready, *Carbon*, **46**, 2026 (2008).
21. H. C. Malecki and M. Zupan, *Compos. Part A-Appl. S.*, **43**, 1914 (2012).
22. Z. H. Fan, M. H. Santare, and S. G. Advani, *Compos. Part A-Appl. S.*, **39**, 540 (2008).
23. N. A. Siddiqui, M. L. Sham, B. Z. Tang, A. Munir, and J. K. Kim, *Compos. Part A-Appl. S.*, **40**, 1606 (2009).
24. D. Domingues, E. Logakis, and A. A. Skordos, *Carbon*, **50**, 2493 (2012).
25. S. Markkula, H. C. Malecki, and M. Zupan, *Compos. Struct.*, **95**, 337 (2013).
26. A. Warrier, A. Godara, O. Rochez, L. Mezzo, F. Luizi, L. Gorbatikh, S. V. Lomov, A. W. VanVuure, and I. Verpoest,

Compos. Part A-Appl. S., **41**, 532 (2010).
27. J. E. Zhang, R. C. Zhuang, J. W. Liu, E. Mader, G. Heinrich, and S. L. Gao, *Carbon*, **48**, 2273 (2010).
28. S. L. Gao, R. C. Zhuang, J. Zhang, J. W. Liu, and E. Mader, *Adv. Funct. Mater.*, **20**, 1885 (2010).
29. N. A. Siddiqui, E. L. Li, M. L. Sham, B. Z. Tang, S. L. Gao, E. Mader, and J. K. Kim, *Compos. Part A-Appl. S.*, **41**, 539 (2010).
30. J. Guo and C. Lu, *Carbon*, **50**, 3101 (2012).
31. J. Guo, C. Lu, F. An, and S. He, *Mater. Lett.*, **66**, 382 (2012).
32. H. Qian, E. S. Greenhalgh, M. S. P. Shaffer, and A. Bismarck, *J. Mater. Chem.*, **20**, 4751 (2010).
33. R. J. Sager, P. J. Klein, D. C. Lagoudas, Q. Zhang, J. Liu, L. Dai, and J. W. Baur, *Compos. Sci. Technol.*, **69**, 898 (2009).
34. J. J. Qiu, C. Zhang, B. Wang, and R. Liang, *Nanotechnology*, **18** (2007).
35. E. F. Reia da Costa, A. A. Skordos, I. K. Partridge, and A. Rezai, *Compos. Part A-Appl. S.*, **43**, 593 (2012).
36. J. D. Schaefer, A. J. Rodriguez, M. E. Guzman, C. S. Lim, and B. Minaie, *Carbon*, **49**, 2750 (2011).
37. A. J. Rodriguez, M. E. Guzman, C.-S. Lim, and B. Minaie, *Carbon*, **49**, 937 (2011).
38. J. Yu, N. Grossiord, C. E. Koning, and J. Loos, *Carbon*, **45**, 618 (2007).
39. Y. Geng, M. Y. Liu, J. Li, X. M. Shi, and J. K. Kim, *Compos. Part A-Appl. S.*, **39**, 1876 (2008).
40. R. Zhang, Y. Huang, L. Liu, Y. Tang, D. Su, and L. Xu, *Mater. Des.*, **33**, 367 (2012).
41. R. L. Zhang, Y. D. Huang, D. Su, L. Liu, and Y. R. Tang, *Mater. Des.*, **34**, 649 (2012).
42. R. L. Zhang, Y. D. Huang, L. Liu, Y. R. Tang, D. Su, and L. W. Xu, *Appl. Surf. Sci.*, **257**, 3519 (2011).
43. R. L. Zhang, Y. D. Huang, L. Liu, Y. R. Tang, D. Su, and L. W. Xu, *Appl. Surf. Sci.*, **257**, 1840 (2011).
44. A. Godara, L. Gorbatikh, G. Kalinka, A. Warrier, O. Rochez, L. Mezzo, F. Luizi, A. W. van Vuure, S. V. Lomov, and I. Verpoest, *Compos. Sci. Technol.*, **70**, 1346 (2010).
45. J. H. Guo, C. X. Lu, and F. An, *J. Mater. Sci.*, **47**, 2831 (2012).
46. X. Li, Y. Qin, S. T. Picraux, and Z.-X. Guo, *J. Mater. Chem.*, **21**, 7527 (2011).
47. S. W. Kim, T. Kim, Y. S. Kim, H. S. Choi, H. J. Lim, S. J. Yang, and C. R. Park, *Carbon*, **50**, 3 (2012).
48. Y. J. Wan, L. C. Tang, D. Yan, L. Zhao, Y. B. Li, L. B. Wu, J. X. Jiang, and G. Q. Lai, *Compos. Sci. Technol.*, **82**, 60 (2013).
49. P. C. Ma, N. A. Siddiqui, G. Marom, and J. K. Kim, *Compos. Part A-Appl. S.*, **41**, 1345 (2010).
50. V. C. Moore, M. S. Strano, E. H. Haroz, R. H. Hauge, R. E. Smalley, J. Schmidt, and Y. Talmon, *Nano Letters*, **3**, 1379 (2003).
51. C. Richard, F. Balavoine, P. Schultz, T. W. Ebbesen, and C. Mioskowski, *Science*, **300**, 775 (2003).
52. H. Gu, S. Tadakamalla, Y. Huang, H. A. Colorado, Z. Luo, N. Haldolaarachchige, D. P. Young, S. Wei, and Z. Guo, *ACS Appl. Mater. Interfaces*, **4**, 5613 (2012).
53. L. C. Tang, X. Wang, Y. J. Wan, L. B. Wu, J. X. Jiang, and G. Q. Lai, *Mater. Chem. Phys.*, **141**, 333 (2013).
54. L. C. Tang, Y. J. Wan, D. Yan, Y. B. Pei, L. Zhao, Y. B. Li, L. B. Wu, J. X. Jiang, and G. Q. Lai, *Carbon*, **60**, 16 (2013).
55. M. Tajvidi, R. H. Falk, and J. C. Hermanson, *J. Appl. Polym. Sci.*, **101**, 4341 (2006).
56. S. Houshyar, R. A. Shanks, and A. Hodzic, *J. Appl. Polym. Sci.*, **96**, 2260 (2005).
57. L. Li, C. Y. Li, and C. Ni, *J. Am. Chem. Soc.*, **128**, 1692 (2006).
58. A. Amash and P. Zugenmaier, *J. Appl. Polym. Sci.*, **63**, 1143 (1997).
59. L. Vaisman, G. Marom, and H. D. Wagner, *Adv. Funct. Mater.*, **16**, 357 (2006).
60. S. Rahmanian, K. S. Thean, A. R. Suraya, M. A. Shazed, M. A. M. Salleh, and H. M. Yusoff, *Mater. Des.*, **43**, 10 (2013).
61. C. R. Chiang, *Compos. Sci. Technol.*, **50**, 479 (1994).
62. S. Y. Fu and B. Lauke, *Compos. Sci. Technol.*, **56**, 1179 (1996).
63. S. Y. Fu and B. Lauke, *Compos. Sci. Technol.*, **58**, 389 (1998).
64. B. Lauke and S.-Y. Fu, *Compos. Sci. Technol.*, **59**, 699 (1999).
65. D. Hull and T. W. Clyne, "An Introduction to Composite Materials", Cambridge: Cambridge University Press, 2001.
66. D. Y. Wu, S. Meure, and D. Solomon, *Prog. Polym. Sci.*, **33**, 479 (2008).
67. S. Y. Fu, B. Lauke, Y. H. Zhang, and Y. W. Mai, *Compos. Part A-Appl. S.*, **36**, 987 (2005).
68. S. Y. Fu, B. Lauke, R. K. Y. Li, and Y. W. Mai, *Compos. Part B-Eng.*, **37**, 182 (2005).